Acta Mathematicae Applicatae Sinica, English Series
Vol. 32, No. 3 (2016) 631–646
DOI: 10.1007/s10255-016-0592-7
http://www.ApplMath.com.cn & www.SpringerLink.com

Acta Mathematicae Applicatae Sinica, English Series

A Nonlinear Diffusion Model for Image Restoration

Yong-gui ZHU†, Xin-yan YU, Bin ZHANG, Xiu-xiu NIU

School of Science, Communication University of China, Beijing 100024, China (E-mail: ygzhu@cuc.edu.cn)

Abstract In this paper, we study the ill posed Perona-Malik equation of image processing[14] and the regularized P-M model i.e. C-model proposed by Catte et al.[4]. The authors present the convex compound of these two models in the form of the system of partial differential equations. The weak solution for the equations is proved in detail. The additive operator splitting (AOS) algorithm for the proposed model is also given. Finally, we show some numeric experimental results on images.

Keywords Perona-Malik model; C-model; weak solutions; AOS algorithm
2000 MR Subject Classification 35R30; 65M06; 65Q05; 65J22

1 Introduction

It is well known that P. Perona and J. Malik[14] have proposed an anisotropic diffusion model for image restoration based on the following partial differential equation:

$$\frac{\partial u}{\partial t} = \operatorname{div}\left(g(|\nabla u|)\nabla u\right), \qquad u|_{t=0} = u_0. \tag{1}$$

In this equation, u_0 is the observed image, u is the original image to be recovered, g is a smooth nonincreasing positive function with $g(0) = 1$, $g(s) \to 0$, at infinity. Its main idea is that the smoothing process obtained by the equation is conditional: if x (x is the image point) is an edge point where $\nabla u(x)$ is large, then the diffusion will be low and therefore the edge will be kept. If x is in homogeneous area, then $\nabla u(x)$ is low and the diffusion will tend to smooth around x. Since an edge stopping function $g(|\nabla u|)$ in the smoothing process is introduced, P-M model has been considered as an important theory of edge detection[12]. The experimental results obtained by Perona and Malik[14] were very impressive, edges remained much more stable across the scales.

However, the Perona-Malik model is ill-posed in mathematics[9]. It has several serious, practical and theoretical difficulties. Indeed if the image is noisy, then the noise produces very large oscillation of the gradient ∇u. Thus the conditional smoothing introduced by the model will not give good results since all these noise edges will be kept. For these difficulties, there have been many people who attempt to study the Perona-Malik equation. And several nonlinear diffusion model have been developed and a sound interpretation can be given in [15,1,13,2,16,5,6,11]. One of the ways to tackle the ill-posed P-M equation is regularizing the term $g(|\nabla u|)$ so as to get a well-posed equation. By reducing the amount of regularization and observing the behavior of the solution of the regularized problem, one can obtain precious information of the initial image. In 1992, F. Catte et al.[4] substituted in the edge function $g(|\nabla u|)$ the gradient of the image ∇u by a smooth version $G_\sigma * \nabla u$, where G_σ is a Gaussian

Manuscript received November 3, 2011. Revised February 6, 2012.
Supported in part by the National Natural Science Foundation of China under Grant (No. 11571325, No. 11271126), Science Research Project of CUC under Grant No. 3132016XNL1612.
†Corresponding author.

smoothing kernel, and obtained the following equation:

$$\begin{cases} \dfrac{\partial u}{\partial t} = \operatorname{div}\big(g(|\nabla G_\sigma * u|)\nabla u(t,x)\big) \\ u|_{t=0} = u_0(x). \end{cases} \tag{2}$$

For the convenence, we call this equation as C-equation or C-Model. In [4], Catte et al. prove the existence, uniqueness and regularity of a solution. For the C-equation, the $G_\sigma * u(x,t)$ is nothing but the solution at scale σ of the heat equation with $u(x,t)$ as initial data. This regularized method belongs to spatial regularization. This model has the advantages over the Perona-Malik model: if the initial image is very noisy, then the Perona-Malik model can't distinguish between "true" edges and "false" edges created by the noise. But the regularized model avoids this drawback, since the equation will diffuse when the gradient is small. In addition, the model makes the filter insensitive to noise at time $t\sigma$, since $(\nabla G_\sigma * u)(t,x)$ is exactly the gradient of the solution at time σ of the solution of the heat equation with initial data $u(t,x)$.

The second regularized method to overcome ill-posed difficulties is time-delay regularization model. The idea of the time-delay regularization has been used in the model of Nitzberg and Shiota[1] at first. This kind of model is very close to the Malik and Perona equation since there is no spatial smoothing. It is described by the following system:

$$\begin{aligned} &\frac{\partial u}{\partial t} = \operatorname{div}\big(g(v)\nabla u(t,x)\big), \qquad u|_{t=0} = u_0(x) \\ &\frac{\partial v}{\partial t} = |\nabla u|^2 - v, \qquad v|_{t=0} = v_0(x). \end{aligned} \tag{3}$$

It is pointed out that time-delay regularization has been used in image processing by diffusion tensors. In 2001, Chen[7] incorporated time-delay regularization into curvature based diffusion model as following:

$$\begin{aligned} &\frac{\partial u}{\partial t} = g(v)|\nabla u|\operatorname{div}\Big(\frac{\nabla u}{|\nabla u|}\Big) + \nabla g(v)\nabla u - \lambda|\nabla u|(u-u_0)), \qquad u|_{t=0} = u_0(x) \\ &\frac{\partial v}{\partial t} = -\frac{1}{\tau}(v - |\nabla G_\sigma * u|^2), \qquad v|_{t=0} = v_0(x). \end{aligned} \tag{4}$$

In which λ is a weighting parameter, G_σ is a Gaussian smoothing kernel with a pre-specified σ. τ is a time-scale factor, $g(s) = \frac{1}{1+Ks}$ with $K > 0$. In [7], Chen showed the existence,uniqueness and stability of the "viscosity" solution of the model. In [8], T. Goldstein and S. Osher proposed split Bregman method and solved the class of L1-regularized problems. They applied this scheme to Rudin-Osher-Fatemi[15] functional for image denoising. In recent, Y. Zhu et al. developed a fast alternating minimization method for MR images in [19] and analyzed the convergence of the method in [20]. In addition, Y. Zhu et al. also gave a fast method for MR images reconstruction in [21] and weighted-average alternating minimization method for MRI reconstruction in [22].

In our work, we develop a new model for image restoration, which is based on the ideas of the delay-time regularization. We will give detailed discussion in the latter sections. Our paper is organized as follows: in the Section 2, we propose the convex incorporation form of P-M equation and C-equation by the view points of the delay-time regularization. In Section 3, we give the proofs of the existence of weak solution for the proposed model. AOS numerical implementation details are discussed in Section 4. Section 5 concludes this paper.

2 The Convex Composition of P-M Equation and C-equation

Let $\Omega \subset R^2$ be the image domain, $\partial\Omega$ denotes the boundary. In this paper, the new developed nonlinear diffusion model is the following system of PDES:

$$\frac{\partial u}{\partial t} = \mathrm{div}\,(g(v)\nabla u), \qquad \frac{\partial u}{\partial n}\Big|_{\partial\Omega} = 0, \qquad u|_{t=0} = u_0(x), \tag{5}$$

$$\frac{\partial v}{\partial t} = (1-\lambda)(|\nabla u| - v) + \lambda \mathrm{div}\,(\nabla v), \qquad \frac{\partial v}{\partial n}\Big|_{\partial\Omega} = 0, \qquad v|_{t=0} = v_0, \tag{6}$$

where u_0 is the observed image to be processed, $g(s) = \frac{1}{1+(\frac{s}{K})^2}$, $0 \le \lambda \le 1$.

Now we can find that when $\lambda = 0$, (6) becomes

$$\frac{\partial v}{\partial t} = |\nabla u| - v.$$

If let $v|_{t=0} = |\nabla u|$, then $v = |\nabla u|$ is the solution for

$$\frac{\partial v}{\partial t} = |\nabla u| - v, \qquad v|_{t=0} = |\nabla u|.$$

Thus (5) becomes $\frac{\partial u}{\partial t} = \mathrm{div}\,(g(|\nabla u|)\nabla u)$, which is the Perona-Malik equation.

When $\lambda = 1$, Equation (6) becomes $\frac{\partial v}{\partial t} = div(\nabla v)$. Let $v|_{t=0} = |\nabla u|$, then $G_\sigma * u(x,t)(\sigma = \sqrt{2t})$ is nothing but the solution for

$$\frac{\partial v}{\partial t} = \mathrm{div}\,(\nabla v), \qquad v|_{t=0} = |\nabla u|.$$

So (5) becomes

$$\frac{\partial u}{\partial t} = \mathrm{div}\,(g(|\nabla G_\sigma * \nabla u|)\nabla u),$$

and which is the regularization of the Perona-Malik model proposed by F. Catte et al.[4]. That is the C-equation as mentioned above.

Since $(1-\lambda)(|\nabla u| - v|) + \lambda \mathrm{div}\,(\nabla v)$ $(0 \le \lambda \le 1)$ is the convex combination of $(|\nabla u| - v)$ and $div(\nabla v)$, we might as well call the system of PDES:

$$\frac{\partial u}{\partial t} = \mathrm{div}\,(g(v)\nabla u), \qquad \frac{\partial v}{\partial t} = (1-\lambda)(|\nabla u| - v) + \lambda \mathrm{div}\,(\nabla v)$$

as the convex composite form of P-M equation and C-equation. In the next section, we will prove the existence of weak solution for the system of PDES (5) and (6).

3 The Existence of Weak Solution for the Proposed PDES Model

Firstly, let us give the proof of the existence of weak solution for the equation (5) i.e.,

$$\frac{\partial u}{\partial t} = \mathrm{div}\,(g(v)\nabla u), \qquad \frac{\partial u}{\partial n}\Big|_{\partial\Omega=0}, \qquad u|_{t=0} = u_0.$$

In 2-dimension, Equation (5) can be rewritten as

$$\frac{\partial u}{\partial t} = \frac{\partial}{\partial x}\Big(g(v)\frac{\partial u}{\partial x}\Big) + \frac{\partial}{\partial y}\Big(g(v)\frac{\partial u}{\partial y}\Big).$$

Assume $0 \le t \le T,\ T > 0$. Let $Q_T = \Omega \times [0, T]$, and it is a cylindrical domain. Discrete the time variable t by the form $t = kh,\ h = \frac{T}{m}$, m is a positive integer. Suppose Ω_k is the intersection of the plane $t = kh$ with Q_T, while S_k is its boundary. On all of the $\Omega_k,\ k = 1, 2, \cdots, m$, we consider the problem

$$u_{\bar{t}}(x, kh) = \operatorname{div}(g^h \nabla u(x, kh)), \qquad \frac{\partial u}{\partial n}\Big|_{\partial\Omega_T = 0} = 0, \qquad u|_{t=0} = u_0, \tag{7}$$

in which

$$u_{\bar{t}}(x, kh) = \frac{1}{h}(u(x, kh) - u(x, kh - h)), \qquad g^h = \frac{1}{h}\int_{kh-h}^{kh} g(v(x, t))\, dt.$$

Obviously, Problem (7) is strictly elliptic, and it is uniquely solvable in $H^1(\Omega)$. Multiply (7) by $2hu(x, kh)$, sum the obtained equality over k from 1 to some $k_0 \le m$ and integrate the resulting over Ω,

$$2h\int_\Omega \sum_{k=1}^{k_0} u(x, kh) u_{\bar{t}}(x, kh) dx = 2h\int_\Omega \sum_{k=1}^{k_0} u(x, kh) \operatorname{div}(g^h \nabla u) dx.$$

Using the integration by parts we can obtain

$$2h\sum_{k=1}^{k_0}\int_{\Omega_k} u_{\bar{t}}(x, kh) u(x, kh) dx + 2h\sum_{k=1}^{k_0}\int_{\Omega_k} g^h |\nabla u(x, kh)|^2 dx = 0. \tag{8}$$

The first term of the above equality can be changed by the following elementary identity:

$$2h\sum_{k=1}^{k_0} u_{\bar{t}}(x, kh) u(x, kh) = u^2(x, k_0 h) - u^2(x, 0) + h^2 \sum_{k=1}^{k_0} \big(u_{\bar{t}}(x, kh)\big)^2. \tag{9}$$

This identity is easily verified. Indeed, since

$$\begin{aligned} 2h\sum_{k=1}^{k_0} u_{\bar{t}}(x, kh) u(x, kh) =& 2h\sum_{k=1}^{k_0} \frac{1}{h}(u(x, kh) - u(x, kh - h)) u(x, kh) \\ =& 2\sum_{k=1}^{k_0} (u^2(x, kh) - u(x, kh - h) u(x, kh)), \end{aligned}$$

while

$$\begin{aligned} & u^2(x, k_0 h) - u^2(x, 0) + h^2 \sum_{k=1}^{k_0} (u_{\bar{t}}(x, kh))^2 \\ =& u^2(x, k_0 h) - u^2(x, 0) + h^2 \sum_{k=1}^{k_0} \Big(\frac{1}{h}(u(x, kh) - u(x, kh - h))\Big)^2 \\ =& u^2(x, k_0 h) - u^2(x, 0) + \sum_{k=1}^{k_0} (u(x, kh) - u(x, kh - h))^2 \\ =& 2\sum_{k=1}^{k_0} (u^2(x, kh) - u(x, kh - h) u(x, kh)). \end{aligned}$$

Thus the identity (9) is true.

Using the identity (9), we can make (8) become

$$\int_\Omega u^2(x,k_0h)dx - \int_\Omega u^2(x,0)dx + h^2\int_\Omega \sum_{k=1}^{k_0}(u_{\bar{t}}(x,kh))^2dx + 2h\int_\Omega \sum_{k=1}^{k_0} g^h|\nabla u(x,kh)|^2dx = 0.$$

That is

$$\int_\Omega u^2(x,k_0h)dx - \int_\Omega u^2(x,0)dx + h^2\sum_{k=1}^{k_0}\int_{\Omega_k}(u_{\bar{t}}(x,kh))^2dx + 2h\sum_{k=1}^{k_0}\int_{\Omega_k} g^h|\nabla u(x,kh)|^2dx = 0.$$

Assume $\nu = \inf\limits_c\{g(c)\} > 0$, then $g^h \geq \nu$. So we have

$$\int_\Omega u^2(x,k_0h)dx + h^2\sum_{k=1}^{k_0}\int_{\Omega_k}(u_{\bar{t}}(x,kh))^2dx + 2\nu h\sum_{k=1}^{k_0}\int_{\Omega_k}|\nabla u(x,kh)|^2dx \leq \int_\Omega u^2(x,0)dx.$$

Let

$$I_h(k_0) = \int_\Omega u^2(x,k_0h)dx + h^2\sum_{k=1}^{k_0}\int_{\Omega_k}(u_{\bar{t}}(x,kh))^2dx + 2\nu h\sum_{k=1}^{k_0}\int_{\Omega_k}|\nabla u(x,kh)|^2dx,$$

then

$$I_h(k_0) \leq ||u_0||_{L^2(\Omega)}, \qquad k_0 = 0,1,2,\cdots,m. \tag{10}$$

Let $\overline{u^h(x,t)} = \sum\limits_{k=1}^{m}\chi^{m,k}(t)u(x,kh-h)$, where $\chi^{m,k}(t)$ denotes the eigenfunction in $[kh-h,kh),\ k=1,2,\cdots,m$, then

$$\begin{aligned}&\overline{u^h(x,t)} \in W_2^{1,0}(Q_T),\\ &\frac{\partial u^h}{\partial n}\Big|_{\partial\Omega_T} = 0,\\ &u^h|_{t=0} = u_0,\end{aligned}$$

where $W_2^{1,0}(Q_T)$ is the Hilbert space with scalar product $(u,v)_{W_2^{1,0}(Q_T)} = \int_{Q_T}(uv + \bigtriangledown u\cdot\bigtriangledown v)dxdt$. By virtue of (10), in $W_2^{1,0}(Q_T)\overline{u^h(x,t)}$ satisfies

$$\Big|\Big|\overline{u^h(x,t)}\Big|\Big|_{L^2(Q_T)} + \Big|\Big|\nabla\overline{u^h(x,t)}\Big|\Big|_{L^2(Q_T)} \leq C, \tag{11}$$

where C is constant. Because of (11) we can choose a sequence $h_l,\ l=1,2\cdots,(h_l\to 0,\ l\to\infty)$, and a function $u\in W_2^{1,0}(Q_T)$ such that $\{\overline{u^{h_l}}(x,t)\}$ and $\{\nabla\overline{u^{h_l}}(x,t)\}$ converge weakly in $L_2(Q_T)$ to u and ∇u respectively, here u is from $W_2^{1,0}(Q_T)$ and $\frac{\partial u}{\partial n}|_{\partial Q_T=0}$.

Next let us show that $u(x,t)$ satisfies the integral equality in the definition of weak solution:

$$\int_{Q_T}\Big(-u\frac{\partial\eta}{\partial t} + g(v)\nabla u\nabla\eta\Big)dxdt - \int_\Omega u_0\eta(x,0)dx = 0,$$

where $\eta\in W_2^{1,1}(Q_T),\ \eta|_T = 0,\ \eta|_{\partial\Omega_T} = 0$. Multiply Equation (7) by $h\eta(x,kh)$, sum the resulting equality over k from 1 to m and integerate over Ω :

$$\int_\Omega\sum_{k=1}^{m}u_{\bar{t}}(x,kh)h\eta(x,kh)dx = \int_\Omega\sum_{k=1}^{m}div(g^h\nabla u)h\eta(x,kh)dx. \tag{12}$$

For the left side of (12), we give an equality

$$h\sum_{k=1}^{m} u_{\bar{t}}(x,kh)\eta(x,kh) = -h\sum_{k=0}^{m-1} u(x,kh)\eta_t(x,kh) + u(x,mh)\eta(x,mh) - u(x,0)\eta(x,0), \quad (13)$$

here $\eta_t(x,kh) = \frac{1}{h}(\eta(x,kh+h) - \eta(x,kh))$. This can be verified directly.

Indeed, since

$$\begin{aligned}
&-h\sum_{k=0}^{m-1} u(x,kh)\eta_t(x,kh)\\
=&-\sum_{k=0}^{m-1} u(x,kh)(\eta(x,kh+h)-\eta(x,kh))\\
=&-u(x,0)\eta(x,h)+u(x,0)\eta(x,0)-u(x,h)\eta(x,2h)+u(x,h)\eta(x,h)\\
&-u(x,2h)\eta(x,3h)+u(x,2h)\eta(x,2h)+\cdots\\
&-u(x,(m-1)h)\eta(x,mh)+u(x,(m-1)h)\eta(x,(m-1)h)),
\end{aligned}$$

we have

$$\begin{aligned}
&-h\sum_{k=0}^{m-1} u(x,kh)\eta_t(x,kh) + u(x,mh)\eta(x,mh) - u(x,0)\eta(x,0)\\
=&\sum_{k=1}^{m}(u(x,kh)-u(x,kh-h))\eta(x,kh),
\end{aligned}$$

while

$$h\sum_{k=1}^{m} u_{\bar{t}}(x,kh)\eta(x,kh) = \sum_{k=1}^{m}(u(x,kh)-u(x,kh-h))\eta(x,kh),$$

so (13) is true.

In this way, (12) can be changed into

$$-h\sum_{k=0}^{m}\int_{\Omega_k} u\eta_t dx - \int_{\Omega} u(x,0)\eta(x,0)dx + h\sum_{k=1}^{m}\int_{\Omega_k} g^h\nabla u\nabla\eta dx = 0,$$

in which we take $\eta(x,t)$ to be equal to zero for $t > mh$. Rewrite it in the form

$$-\int_{\Omega_T}\overline{u^h(x,t)\eta_t(x,t)} - \int_{\Omega} u(x,0)\eta(x,0)dx + \int_h^T\int_{\Omega}\overline{g^h}\ \overline{\nabla u^h}\overline{\nabla\eta}dxdt = 0,$$

where the line over functions denotes that at the point (x,t) of each layer $x\in\overline{\Omega},\ t\in[kh-h,kh]$ the function is equal to its value at the point $(x,kh-h)$. The piece-wise-continuous functions $\overline{\eta(x,t)}$ and $\overline{\eta_t(x,t)}$ converge uniformly to a continuous differentiable function $\eta(x,t)$ and its derivative $\frac{\partial\eta(x,t)}{\partial t}$. Because $|g(v)|\le 1$, we can choose from $\{h_l\}$ a subsequence $\{h_{l_p}\},\ p=1,2,\cdots$, such that

$$g^{h_{l_p}}(v)\to g(v), \qquad p\to\infty.$$

In view of this and the weak convergence of the $\overline{u^h(x,t)}$ and $\nabla\overline{u^h(x,t)}$ to u and ∇u, we can get

$$\int_{Q_T}\Big(-u\frac{\partial\eta}{\partial t} + g(v)\nabla u\nabla\eta\Big)dxdt - \int_{\Omega} u(x,0)\eta(x,0)dx = 0.$$

This shows that u is the weak solution of Equation (5) in $W_2^{1,0}(Q_T)$.

Now we prove the existence of weak solutions of Equation (6):

$$\frac{\partial v}{\partial t} = (1-\lambda)(|\nabla u| - v) + \lambda \mathrm{div}\,(\nabla v), \qquad v|_{t=0} = v_0, \qquad \frac{\partial v}{\partial n}\Big|_{\partial\Omega} = 0.$$

Similar to the proof of the existence of weak solution for Equation (5), on all the Ω_k, $k = 1, 2, \cdots, m$, we consider the problem:

$$v_{\bar{t}}(x,kh) = (1-\lambda)(|\nabla u^h| - v(x,kh)) + \lambda \mathrm{div}\,(\nabla v(x,kh)), \quad \frac{\partial v}{\partial n}\Big|_{\partial\Omega_T} = 0, \quad v|_{t=0} = v_0, \quad (14)$$

where $v_{\bar{t}}(x,kh) = \frac{1}{h}(v(x,kh) - v(x,kh-h))$, $u^h = \frac{1}{h}\int_{kh-h}^{kh} u(x,t)dt$. Equation (14) is a strictly elliptic problem, and we can see it has the weak solution in $H^1(\Omega)$.

Multiply (14) by $2hv(x,kh)$ and sum the resulting equality over k from 1 to some $k_0 \le m$, and integrate the obtained equality over Ω and have:

$$\begin{aligned} 2h\int_\Omega \sum_{k=1}^{k_0} v(x,kh)v_{\bar{t}}(x,kh)dx =& 2h(1-\lambda)\int_\Omega \Big(\sum_{k=1}^{k_0}(|\nabla u^h|v(x,kh) - v^2(x,kh)\Big)dx \\ &+ 2h\lambda\int_\Omega \Big(\sum_{k=1}^{k_0}\mathrm{div}\,(\nabla v(x,kh))v(x,kh)\Big)dx. \end{aligned}$$

Using the integration by parts, we have

$$\begin{aligned} &2h\sum_{k=1}^{k_0}\int_\Omega v_{\bar{t}}(x,kh)v(x,kh)dx + 2h\lambda\sum_{k=1}^{k_0}\int_\Omega |\nabla v(x,kh)|^2 dx \\ =&2h(1-\lambda)\sum_{k=1}^{k_0}\int_\Omega |\nabla u^h|v(x,kh)dx - 2h(1-\lambda)\sum_{k=1}^{k_0}\int_\Omega |v(x,kh)|^2 dx \\ \le&h(1-\lambda)\sum_{k=1}^{k_0}\int_\Omega |\nabla u^h|^2 dx + h(1-\lambda)\sum_{k=1}^{k_0}\int_\Omega |v(x,kh)|^2 dx - 2h(1-\lambda)\sum_{k=1}^{k_0}\int_\Omega |v(x,kh)|^2 dx \\ =&h(1-\lambda)\sum_{k=1}^{k_0}\int_{\Omega_k} |\nabla u^h|^2 dx - h(1-\lambda)\sum_{k=1}^{k_0}\int_\Omega |v(x,kh)|^2 dx. \end{aligned}$$

That is

$$\begin{aligned} &2h\sum_{k=1}^{k_0}\int_\Omega v_{\bar{t}}(x,kh)v(x,kh)dx + 2h\lambda\sum_{k=1}^{k_0}\int_{\Omega_k} |\nabla v(x,kh)|^2 dx + h(1-\lambda)\sum_{k=1}^{k_0}\int_{\Omega_k} |v(x,kh)|^2 dx \\ \le&h(1-\lambda)\sum_{k=1}^{k_0}\int_\Omega |\nabla u^h|^2 dx. \end{aligned}$$

Using the elementary identity

$$2h\sum_{k=1}^{k_0} v_{\bar{t}}(x,kh)v(x,kh) = v^2(x,k_0h) - v^2(x,0) + h^2\sum_{k=1}^{k_0}\big(v_{\bar{t}}(x,kh)\big)^2,$$

we can obtain

$$\begin{aligned}&\int_\Omega v^2(x,k_0h)dx-\int_\Omega v^2(x,0)dx+h^2\int_\Omega\sum_{k=1}^{k_0}(v_{\bar t}(x,kh))^2dx\\&+2h\lambda\sum_{k=1}^{k_0}\int_{\Omega_k}|\nabla v(x,kh)|^2dx+h(1-\lambda)\sum_{k=1}^{k_0}\int_{\Omega_k}|v(x,kh)|^2dx\\\le&h(1-\lambda)\sum_{k=1}^{k_0}\int_{\Omega_k}|\nabla u^h|^2dx.\end{aligned}$$

That is

$$\begin{aligned}&\int_\Omega v^2(x,k_0h)dx+h^2\sum_{k=1}^{k_0}\int_{\Omega_k}(v_{\bar t}(x,kh))^2dx+2h\lambda\sum_{k=1}^{k_0}\int_{\Omega_k}|\nabla v(x,kh)|^2dx\\\le&h(1-\lambda)\sum_{k=1}^{k_0}\int_{\Omega_k}|\nabla u^h|^2dx+\int_\Omega v^2(x,0)dx-h(1-\lambda)\sum_{k=1}^{k_0}\int_{\Omega_k}|v|^2dx\\\le&h(1-\lambda)\sum_{k=1}^{k_0}\int_{\Omega_k}|\nabla u^h|^2dx+\int_\Omega v^2(x,0)dx.\end{aligned}$$

Let

$$J_h(k_0)=\int_\Omega v^2(x,k_0h)dx+h^2\sum_{k=1}^{k_0}\int_{\Omega_k}(v_{\bar t}(x,kh))^2dx+2h\lambda\sum_{k=1}^{k_0}\int_{\Omega_k}|\nabla v(x,kh)|^2dx,$$

then

$$J_h(k_0)\le c\big(||\nabla u||^2_{L^2(Q_{k_0h})}+||v_0||^2_{L^2(\Omega)}\big),\qquad K_0=0,1,2,\cdots,m.\tag{15}$$

If assume

$$\overline{v^h(x,t)}=\sum_{k=1}^{m}\chi^{m,k}(t)v(x,kh-h),$$

where $\chi^{m,k}(t)$ is the eigenfunction on $[kh-h,kh),\ k=1,2,\cdots,m$, then

$$\overline{v^h(x,t)}\in W_2^{1,0}(Q_T),\qquad \frac{\partial v^h}{\partial n}\Big|_{\partial Q_T}=0,\qquad v^h|_{t=0}=v_0.$$

We can obtain from (15) that the function $\overline{v^h(x,t)}$ have uniformly bounded norms in $W_2^{1,0}(Q_T)$:

$$\|\overline{v^h}\|_{L^2(Q_T)}+\|\nabla\overline{v^h}\|_{L^2(Q_T)}\le c_1.\tag{16}$$

Because of (16), a sequence $h_l,\ l=1,2,\cdots,\ (h_l\to0,\ l\to\infty)$ and a function $v\in W_2^{1,0}(Q_T)$ can be chosen such that $\{\overline{v_l^h(x,t)}\}$ and $\{\nabla\overline{v_l^h(x,t)}\}$ converge weakly in $L_2(Q_T)$ to v and ∇v respectively. In which, v is from $W_2^{1,0}(Q_T)$, and $\frac{\partial v}{\partial n}\big|_{\partial Q_T}=0$.

Now we prove that $v(x,t)$ is a weak solution i.e. it satisfies the following integral equality:

$$\int_{Q_T}\Big(-v\frac{\partial\eta}{\partial t}+\lambda\nabla v\nabla\eta\Big)dxdt-\int_\Omega v_0\eta(x,0)dx=(1-\lambda)\int_{Q_T}(|\nabla u|-v)\eta dxdt,$$

where $\eta \in W_2^{1,1}(Q_T),\ \eta|_{t=T} = 0,\ \eta|_{\partial Q_T} = 0$. Multiply Equation (14) by $h\eta(x,kh)$, sum the obtained equality over k from 1 to m and integrate over Ω :

$$\int_\Omega \sum_{k=1}^{m} v_t(x,kh)h\eta(x,kh)dx = (1-\lambda)\int_\Omega \sum_{k=1}^{m}(|\nabla u^h| - v(x,kh)h\eta(x,kh)dx + \lambda\int_\Omega \sum_{k=1}^{m} \operatorname{div}(\nabla v(x,kh))h\eta(x,kh)dx. \tag{17}$$

We transform the left term of Equality (17) by means of the following formula:

$$h\sum_{k=1}^{m} v_{\bar{t}}(x,kh)\eta(x,kh) = -h\sum_{k=0}^{m-1} v(x,kh)\eta_t(x,kh) + v(x,mh)\eta(x,mh) - v(x,0)\eta(x,0), \tag{18}$$

in which $\eta_t(x,kh) = \frac{1}{h}(\eta(x,kh+h) - \eta(x,kh))$. The proof of this equality is similar to Equality (13). So (17) can become

$$\begin{aligned} &-h\sum_{k=0}^{m}\int_{\Omega_k} v\eta_t dx - \int v(x,0)\eta(x,0)dx + h\lambda\sum_{k=1}^{m}\int_{\Omega_k}\nabla v\nabla\eta dx \\ =&(1-\lambda)h\sum_{k=1}^{m}\int_{\Omega_k}(|\nabla u^h| - v(x,kh))\eta dx, \end{aligned}$$

where $\eta(x,t) = 0$, when $t > mh$. Let us rewrite it in the form:

$$\begin{aligned} &-\int_{Q_T}\overline{v^h(x,t)}\ \overline{\eta_t(x,t)}dxdt - \int_\Omega v(x,0)\eta(x,0)dx + \lambda\int_n^T\int_\Omega \nabla\overline{v^h}\ \nabla\overline{\eta}dxdt \\ =&(1-\lambda)\int_h^T\int_\Omega(|\nabla\overline{u^h}| - \overline{v(x,t)})\overline{\eta(x,t)}dxdt, \end{aligned}$$

in which the line over some of the functions means that at the point (x,t) of each layer $x \in \overline{\Omega},\ t \in [kh-h, kh)$ the function is the value at the point $(x, kh-h)$.

For a continuously differentiable function $\eta(x,t)$, the piecewise-continuous functions $\overline{\eta(x,t)}$ converge uniformly to $\eta(x,t)$, while the functions $\overline{\eta_t(x,t)}$ approximate to its derivative $\frac{\partial\eta}{\partial t}$. Because $\overline{u^h(x,t)}$ and $\nabla\overline{v^h(x,t)}$ converge weakly to v and ∇v, we can obtain

$$\int_{Q_T}\Big(-v\frac{\partial\eta}{\partial t}\Big)dxdt - \int_\Omega v(x,0)\eta(x,0)dx + \lambda\int_{Q_T}\nabla v\nabla\eta dxdt = (1-\lambda)\int_{Q_T}(|\nabla u| - v)\eta dxdt.$$

This equality shows that v is the weak solution of Equality (6) in $W_2^{1,0}(Q_T)$.

Based on the above results, we can give the following theorem.

Theorem 1. *Let $T > 0,\ Q_T = \Omega \times [0,T]$. If $u_0 \in H^1(\Omega)$, then PDES system:*

$$\frac{\partial u}{\partial t} = div(g(v)\nabla u), \qquad \frac{\partial u}{\partial n}\Big| = 0, \qquad u|_{t=0} = u_0, \tag{19}$$

$$\frac{\partial v}{\partial t} = (1-\lambda)(|\nabla u| - v) + \lambda div(\nabla v), \qquad \frac{\partial v}{\partial n}\Big|_{\partial\Omega} = 0, \qquad v|_{t=0} = v_0, \tag{20}$$

has a weak solution (u,v) in $\big(W_2^{1,0}(Q_T)\big) \times \big(W_2^{1,0}(Q_T)\big)$. In which

$$g(s) = \frac{1}{1+\frac{s^2}{K^2}}, \qquad 0 \le \lambda \le 1.$$

4 Numerical Scheme and Experimental Results

To solve our proposed model, we use an semi-implicit additive operator splitting (AOS) scheme (see [17,18,10,3]). Now we describe the numerical method used to implement our model. A discrete image can be regarded as a vector $f \in R^N$, whose components $f_i,\ i \in \{1, 2, \cdots, N\}$ display the grey values at each pixel. Pixel i represents the location x_i. In the following discussion, we use h_l to denote the grid size in the l $(l = 1, 2)$ direction. Consider discrete times $t_k = k\tau$, where $k \in N_0$ and τ is the time step size, we use u_i^k and g_i^k to denote the approximations to $u(x_i, t_k)$ and $g(v(x_i, t_k))$ respectively. A semi-implicit discrete scheme for Equation (19) with Neumann boundary conditions is given by $\frac{u_i^{k+1}-u_i^k}{\tau} = \sum_{l=1}^{2} \sum_{j\in N_l(i)} \frac{g_j^k+g_i^k}{2h_l^2}(u_j^{k+1} - u_i^k)$, where $N_l(i)$ consists of the two neighbors of pixel i along the l direction (boundary pixels may have only one neighbor). We can rewrite the semi-implicit scheme in pix-vector notation as $\frac{u^{k+1}-u^k}{\tau} = A_l(u^k)u^{k+1}$ $(l = 1, 2)$, with $A_l(u^k) = \big(a_{ijl}(u^k)\big)$ and

$$a_{ijl}(u^k) = \begin{cases} \dfrac{g_i^k + g_j^k}{2h_l^2}, & j \in N_l(j), \\ -\displaystyle\sum_{n\in N_l(i)} \dfrac{g_i^k + g_h^k}{2h_l^2}, & j = i, \\ 0, & \text{else.} \end{cases}$$

Solving for u^{k+1} yields

$$u^{k+1} = \Big(I - \tau \sum_{l=1}^{2} A_l(u^k)\Big)^{-1} u^k. \tag{21}$$

According to the AOS approximation idea [17], we can get the AOS scheme for (19):

$$u^{k+1} = \frac{1}{2} \sum_{l=1}^{2} \Big(I - 2\tau \sum_{l=1}^{2} A_l(u^k)\Big)^{-1} u^k. \tag{22}$$

In the same way, we can give the AOS scheme for (20). In matrix-vector notation, a semi-implicit discretization of (20) is given by

$$\frac{v^{k+1} - v^k}{\tau} = (1 - \lambda)(|\nabla u^{k+1}| - v^{k+1}) + \lambda \sum_{l=1}^{2} B_l(v^k)v^{k+1}.$$

Thus v^{k+1} can be given by

$$v^{k+1} = \Big(I - \frac{\lambda\tau}{1 + (1 - \lambda)} \sum_{l=1}^{2} B_l(v^k)\Big)^{-1} \Big(\frac{(1 - \lambda)\tau}{1 + (1 - \lambda)\tau} |\nabla u^{k+1}| + \frac{v^k}{1 + (1 - \lambda)\tau}\Big). \tag{23}$$

So the AOS approximation for (20) is

$$v^{k+1} = \frac{1}{2} \sum_{l=1}^{2} \Big(I - \frac{2\lambda\tau}{1 + (1 - \lambda)\tau} B_l(v^k)\Big)^{-1} \Big(\frac{(1 - \lambda)\tau}{1 + (1 - \lambda)\tau} |\nabla u^{k+1}| + \frac{v^k}{1 + (1 - \lambda)\tau}\Big). \tag{24}$$

Now we can using the above-mentioned AOS scheme to implement our proposed model. The algorithm to implement the proposed PDES system is as follows:

Step 1. Fix iteration numbers N, the value of K, and the grid size h_l $(l = 1, 2)$.
Step 2. Initialize u and v, let $k = 0,\ u = u_0,\ v_0 = |\nabla u_0|$.
Step 3. Using (22) to compute u^{k+1} and give $|\nabla u^{k+1}|$, while v^{k+1} is computed by (24).
Step 4. If $k \leq N$, then End else next step.
Step 5. $k = k + 1$ goto Step 3.

For the complexity of AOS algorithms, we don't discuss it here. The interested readers can refer to [17] for the detailed discussion of the complexity for AOS algorithms. We use Peak-Signal-Noise-Rate(PSNR) and Root-Mean-Square-Error (RMSE) to compare the advantages and disadvantages between our model and C-model or P-M model. PSNR and RMSE is defined by the following:

$$\mathrm{PSNR}(u, w) = 10 \log 10 \frac{255^2}{\frac{1}{mn} \sum_{i,j} (u_{i,j} - w_{i,j})^2}, \tag{25}$$

$$\mathrm{RMSE}(u, w) = \sqrt{\frac{1}{mn} \sum_{i,j} (u_{i,j} - w_{i,j})^2}, \tag{26}$$

where $w_{i,j}$ and $u_{i,j}$ denotes the pixel values of the processed and the original images respectively. In the following examples, we assume $h_l = 1,\ l = 1, 2,\ K = 10$.

Example 1. After the original Lena image is added by the Gaussian white noise with variance $\sigma = 35$, the noisy image can be regarded as an observed image, i.e. u_0 in the model. Let $v_0 = |\nabla u_0|$, and the approximation of $\frac{\partial u_0}{\partial x}$ and $\frac{\partial u_0}{\partial y}$ in $|\nabla u_0|$ is given by the following:

$$\left.\frac{\partial u_0}{\partial x}\right|_{i,j} = \gamma \frac{u_{0i+1,j} - u_{0i-1,j}}{2} + \frac{(1-\gamma)}{2}\Big(\frac{u_{0i+1,j+1} - u_{0i-1,j+1}}{2} + \frac{u_{0i+1,j-1} - u_{0i-1,j-1}}{2}\Big),$$

$$\left.\frac{\partial u_0}{\partial y}\right|_{i,j} = \gamma \frac{u_{0i,j+1} - u_{0i,j-1}}{2} + \frac{(1-\gamma)}{2}\Big(\frac{u_{0i+1,j+1} - u_{0i+1,j-1}}{2} + \frac{u_{0i-1,j+1} - u_{0i-1,j-1}}{2}\Big),$$

where γ is a parameter to be chosen. According to [3], using the above mentioned formula not only keep rotation-invariance properties, but also make the result less sensitive to noise. The computation of $|\nabla u^{k+1}|$ is similar to $|\nabla u_0|$.

Fig. 1(a) is the original image, Fig. 1(b) is the noisy image corrupted by white Gaussian noise with standard deviation $\sigma = 35$. Fig. 1(c) is v_0 that equals to the norm of the gradient of u_0 i. e. Fig. 1(b).

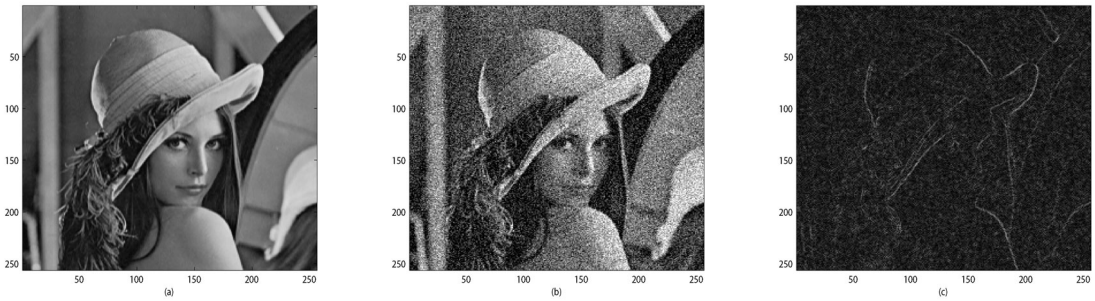

Fig. 1. Lena image. (a) Original image. (b) Noisy image with $\sigma = 35$. (c) Norm of the gradient of noisy image.

In our test, we choose $\lambda = 0.75,\ \gamma = \sqrt{2} - 1$, N (number of iteration)=12. In order to show the better of our method, we compare it with P-M model and C-Model. Fig. 2(a) is the

result of P-M method, Fig. 2(b) is the result of C-model method, and Fig. 2(c) gives the result processed by our method. From the visual quality, Fig. 2(c) is better than Fig. 2(a) and Fig. 2(b).

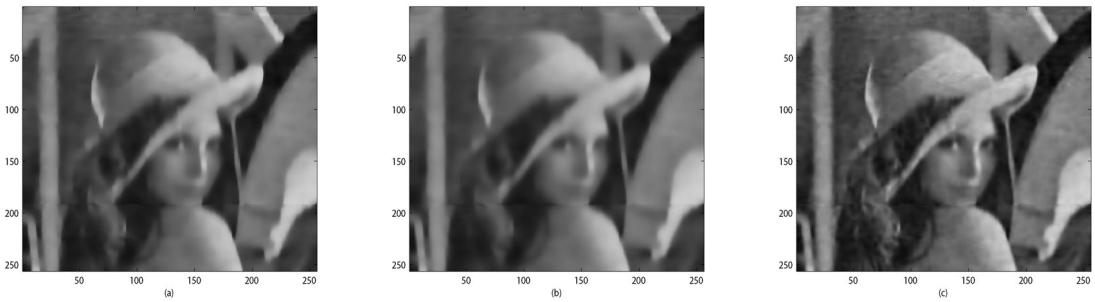

Fig. 2. Results for the Lena Image. (a) P-M Method. (b) C-model Method (c) Our Method.

From all the three restored image, it is clear that our proposed model suppresses more noise while preserves more fine details and small structures in the image. In addition, from the values of PSNR and RMSE for restored image, our method increases the PSNR by 1.5–2.5 dB and reduce the RMSE 2.5–4.0. We report the PSNR and RMSE for each of the schemes in Table I.

Table 1. PSNR and RMSE for each of the SCHEMS

model	P-M model	C-model	our model
PSNR	23.8422 dB	23.1465 dB	25.2917 dB
RMSE	16.3844	17.7506	13.8662

Example 2. A fingerprint image is used in the second test. It is added by the white Gaussian noise with the standard deviation $\sigma = 45$. We choose noisy image and the norm of its gradient as u_0 and v_0. Let iteration number N=16, the values of other parameters are still equal to the corresponding values in Example 1. Using our model, P-M model and C-model to process u_0, we can find that our method is also better than other two methods. Fig. 3(a) is the original image, Fig. 3(b) is the noisy image and Fig. 3(c) is the norm of the gradient of the noisy image. Fig. 4 (a), (b), and (c) show the results processed by the three methods.

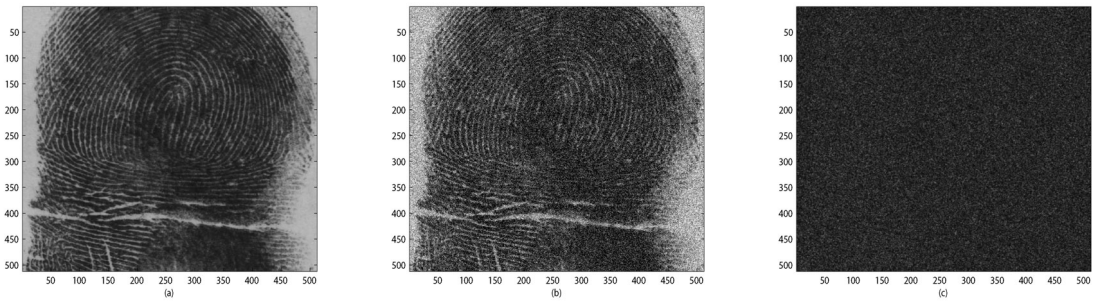

Fig. 3. Fingerprint image. (a) Original image. (b) Noisy image with $\sigma = 45$. (c) Norm of the gradient of noisy image.

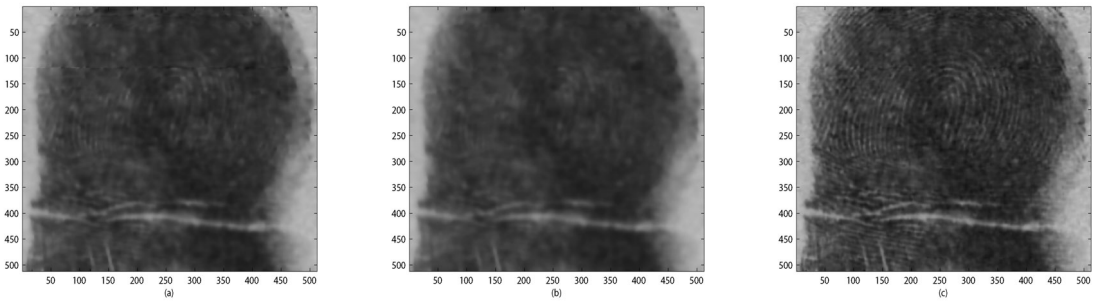

Fig. 4. Results for the fingerprint image. (a) P-M method. (b) C-model method (c) Our method.

Table 2. is the comparison of the values of PSNR and RMSE for restored images.

Table 2. PSNR and RMSE for Restored Images

model	P-M model	C-model	our model
PSNR	23.1576 dB	22.8225 dB	24.4604 dB
RMSE	17.7280	18.4254	15.2588

From the results above, it is obvious that not only for visual quality of images, but also for quantitative evaluation of restored images, our method in texture image processing is still better than other two models.

Example 3. We use an woman image containing both a human face and some textures to do the third test. The challenge with this image is to keep both texture details and smooth transitions in the human face in the processing. We add the original image (Fig. 5(a)) with the white Gaussian noise with $\sigma = 15$, and get a noisy image (Fig. 5(b)). Fig. 5(c) is the norm of the gradient of the noisy image. Fig. 6(a),(b), and (c) are the results obtained by three methods.

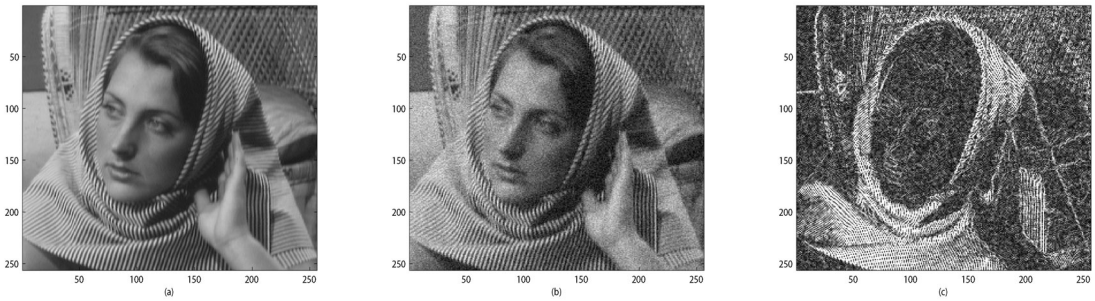

Fig. 5. Woman image. (a) Original image. (b) Noisy image with $\sigma = 15$. (c) Norm of the gradient of noisy image.

Table 3. Comparison of Psnr and Rmse for Restored Images

model	P-M model	C-model	our model
PSNR	21.8072 dB	21.4664 dB	22.7290 dB
RMSE	20.7099	21.5386	18.6248

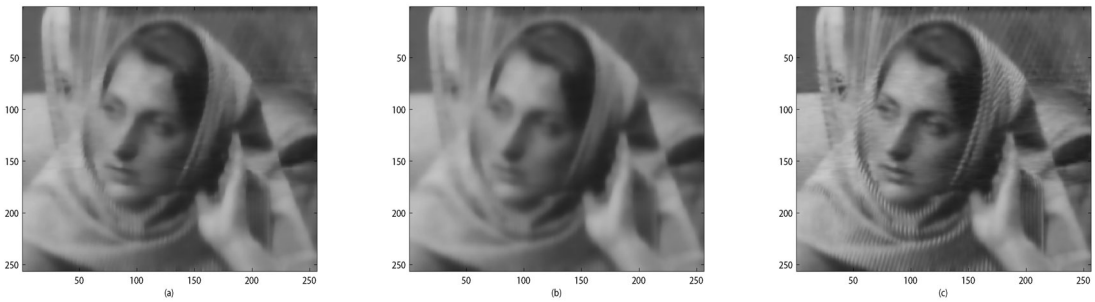

Fig. 6. Results for the woman image. (a) P-M method. (b) C-model method (c) Our method.

In the computation above, we choose the number of iteration is 8. And the values of other parameters are the same as in Example 1. Next table is the quantitative comparison among the three methods.

The results above reveal that our method not only maintain more texture details and smooth transitions in the face but also suppress more noise than other methods after processing. Additionally, our model can increase more PSNR and decrease RESE than P-M model and C-model.

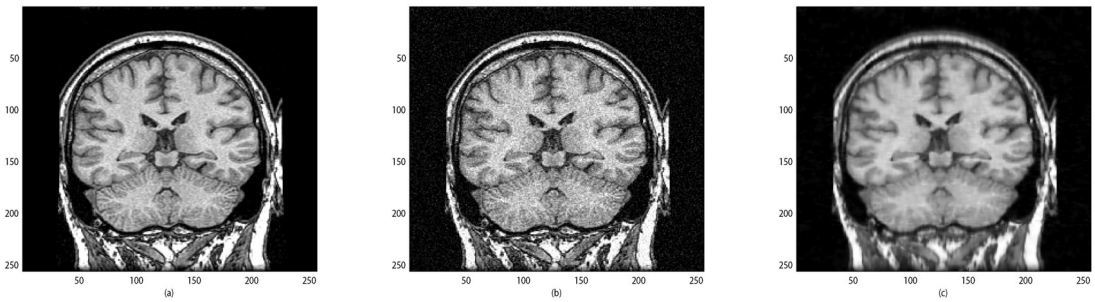

Fig. 7. MR image. (a) Original image. (b) Noisy image with $\sigma = 15$. (c) The result recovered with our scheme.

Fig. 8(a), (b) and (c) are an original remote sensing image, the noisy image, and the processed result by our method. We can see that the recovered image coincides with the true one almost everywhere.

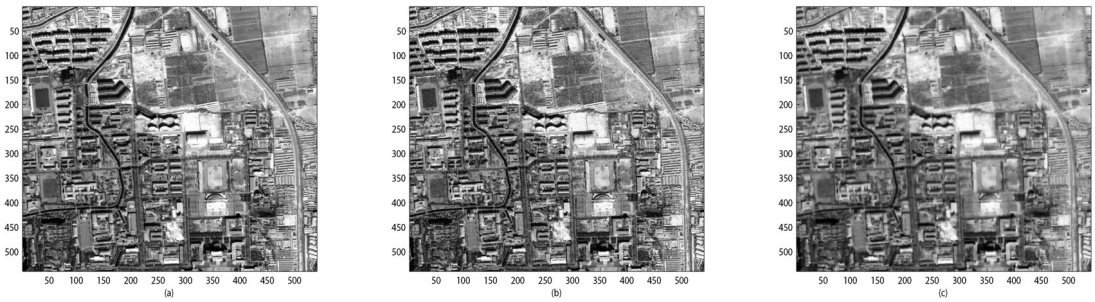

Fig. 8. Remote sensing image. (a) Original image. (b) Noisy image with $\sigma = 20$. (c) The result recovered with our scheme.

At last, we will show some more restored images, which are from a MR image, a remote sensing image, and Canaletto image. And we will only give results recovered by our method. A

MR image (see Fig. 7(a)) has been corrupted with white Gaussian noise ($\sigma = 20$) and become a noisy image, see Fig. 7(b). After the noisy image has been processed with our model, we can see that our restoration scheme is able to maintain all important information and filter out much noise, see Fig. 7(c).

The Canaletto image was used in an article[1] by P. Perona and J. Malik. Malik digitized the image from a small reproduction of the original, which hangs in the National Gallery in Washington, D.C. and was painted in Venice by Antonio Canal, nicknamed 'Canaletto," in 1720. Here we use the Canaletto image again in the test. Fig. 9(a)–(c) are the original image, the noisy image with $\sigma = 20$, and the recovered result with our scheme. From the visual quality, it is obvious that restored image is as good as the original one.

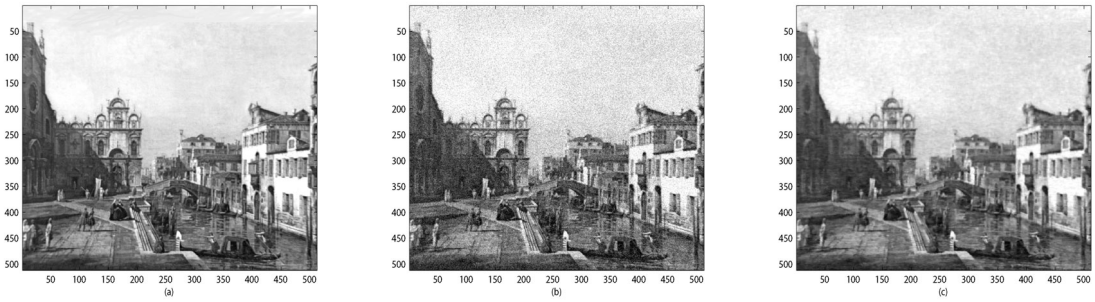

Fig. 9. Canaletto image. (a) Original image. (b) Noisy image with $\sigma = 20$. (c) The result recovered by our scheme.

5 Conclusion

We have developed a new nonlinear diffusion model for image denoising and edge detection. It is the convex combination of C-model and P-M model. Our model can be regarded as a general case of C-model or P-M model. It detects and preserves edges better and also preserves fine details and small structures in the image than C-model and P-M model. We give the proof of the existence of weak solutions for $PDES$ system. The numerical experiments also demonstrate by using the AOS algorithm that our method yields better smoothing and edge detection results and has higher PSNR and less RMSE than other two methods.

Our model can be applied in many kinds of image processing. It can be used in texture image, biomedical images such as MR, CT images processing. Our method can also reduce noises for SAR images and remote sensing images.

References

[1] Alvarez, L., Lions, P.L., Morel, J.M. Image selective smoothing and edge detection by nonlinear diffusion Ⅱ. *SIAM J. Numer. Anal.*, 29(3): 845–866 (1992)
[2] Alvarez, L., Mazorra, L. Signal and image restoration using shock filters and anisotropic diffusion. *SIAM J. Numer. Anal.*, 31(2): 590–605 (1994)
[3] Aubert, G., Kornprobst, P. Mathematical Problems in Image Processing: Partial Differential Equations and the Calculus of Variations, Second Edition. Springer-Verlag, New York, 2006
[4] Catte, F., Lions, P.L., Morel, J.M., Coll, T. Image selective smoothing and edge detection by nonlinear diffusion. *SIAM Journal of Numerical Analysis*, 29(1): 182–193 (1992)
[5] Cottet, G.H., El Ayyadi, M. A Volterra type model for image processing. *IEEE Trans. Image Processing*, 7(3): 292–303 (1998)
[6] Chen, Y.M., Vemuri, B.C., Wang, L. Image denoising and and segmentation via nonlinear diffusion. *International Journal Computers & Mathematics with Applications*, 39(5-6): 131–149 (2000)
[7] Chen, Y.M., Bose, P. On the incorporation of time-delay regularization into curvature-based diffusion. *Journal of Mathematical Imaging and Vision*, 14(2): 149–164 (2001)
[8] Goldstein, T., osher, S. The split Bregman method for L_1-regularized problems. *SIAM J. Image Sciences.* 2(2): 323–343 (2009)
[9] Kichenassamy, S. The Perona-Malik paradox. *SIAM J. Appl. Math.*, 57(5): 1328–1342 (1997)

[10] Krishnan, D., Lin, P., Tai, X.C. An efficient operator-splitting method for noise removal in images. *Commun. Comput. Phys.*, 1(5): 847–858 (2006)
[11] Lysaker, M., Lundervold, A., Tai, X.C Noise removal using fourth-order partial differential equation with applications to medical magnetic resonance images in space and time. *IEEE Trans. Image Processing*, 12(12): 1579–1590 (2003)
[12] Marr, D., Hildreth, E. Theory of edge detection. *In Roy. Soc.*, 207 of B: 187–217 (1980)
[13] Nitzberg, M., Shiota, T. Nonlinear image filtering with edge and corner enhancement. *IEEE Trans. Pattern Anal. and Machine Intelligence*, 14(8): 826–833 (1992)
[14] Perona, P., Malik, J. Scale-space and edge detection using anisotropic diffusion. *IEEE Trans. Pattern Anal. Machine Intell.*, 12(7): 629–639 (1990)
[15] Rudin, L., Osher, S., Fatemi, E. Nonlinear total variation based noise removal algorithms. *Physics D*, 60(1–4): 259–268 (1992)
[16] Weickert, J. Anisotropic diffusion in image processing. B.G. Teubner, Stutgart, 1998
[17] Weickert, J., Romeny, B.M., Viergever, M.A. Efficient and reliable schemes for nonlinear diffusion filtering, *IEEE Trans. Image Processing*, 7(3): 398–410 (1998)
[18] Weickert, J. Applications of nonlinear diffusion in image processing and computer vision. *Acta Math. Univ. Comenianae*, LXX(1): 33–50, Proceedings of Algorithmy (2000)
[19] Zhu, Y., Chern, I. Fast alternating minimization method for compressive sensing MRI under wavelet sparsity and TV sparsity. 2011 Sixth International Conference on Image and Graphics. 356–361, 2011
[20] Zhu, Y., Chern, I. Convergence of the alternating minimization method for sparse MR image reconstruction. *Journal of Information and Computational Science*, 8(11): 2067–2075 (2011)
[21] Zhu, Y., Shi, Y. A fast method for reconstruction of total-variation MR images with a periodic boundary condition. *IEEE signal processing letters*, 20(11): 291–294 (2013)
[22] Zhu, Y., Shi, Y., Zhang, B., Yu, X. Weighted-average alternating minimization method for magnetic resonance image reconstruction based on compressive sensing. *Inverse problems and imaging*, 8(3): 925–937 (2014)